Performance Enhancement of a High-Resolution Pressure Sensor

Milind Singh

Supervised by Professor Laurent Mydlarski

Department of Mechanical Engineering

McGill University

A thesis submitted to McGill University in partial fulfilment of the requirements of the Undergraduate Honours Program.

Abstract

The present work focuses on the performance enhancement of a high-resolution static pressure probe. Physical enhancements are made to the pressure probe to improve its signal-to-noise ratio (SNR). Signal conditioning of the probe results in an improved SNR and it is also observed that low energy fluctuations in static pressure are better resolved using high gain settings. Introducing the probe into a planar jet further improves the SNR as external flow conditions are more optimized for microphone measurements than internal flow conditions. Vibration reduction of the probe is effective in eliminating noise levels in the inertial subrange of the pressure spectra. Improvements in the quality of the recorded pressure spectra are also observed by increasing the fan speed of the channel. Overall noise reduction and increased signal levels result in improvements in the SNR of the probe, as expected. Optimal digital filtering does not, however, effectively isolate the noise contaminating the pressure measurements made by the probe. Measurements need to be made where the noise levels are known to be well correlated to make further conclusions regarding this technique. An alternate method for measuring static pressure is investigated by making simultaneous velocity and total pressure measurements. This method requires further work as there is a remarkable similarity to be observed in the overall shape of the dynamic and static pressures, which should not be the case.

Résumé

Ce travail se concentre sur l'amélioration de la performance d'une sonde de pression statique à haute résolution. Des améliorations physiques à la sonde de pression sont effectués pour améliorer son rapport signal sur bruit (RSB). Le conditionnement du signal de la sonde permet d'améliorer le RSB et on peut également observer que les variations de pression statique avec peu d'énergie ont une meilleure résolution quand des gains élevés sont utilisé. L'introduction de la sonde dans un jet plan améliore davantage le RSB car l'écoulement externe est mieux optimisé pour des mesures de microphone que l'écoulement interne. Diminuer les vibrations de la sonde aide à éliminer les niveaux de bruit dans le sous-domaine inertiel du spectre de pression. La qualité des spectres de pression enregistrés est aussi améliorée quand la vitesse du ventilateur du tunnel aérodynamique est augmentée. Une réduction globale du bruit et une augmentation des niveaux de signal se traduit dans une amélioration du RSB de la sonde, tel qu'anticipé. Cependant, le filtrage numérique optimal ne permet pas d'isoler efficacement le bruit qui contamine les mesures de pression de la sonde. Des mesures doivent être prises là où les niveaux de bruit ont une forte corrélation afin de tirer des conclusions supplémentaires concernant cette technique. Une autre méthode pour mesurer la pression statique, en effectuant simultanément des mesures de vitesse et de pression totale, est étudié. Cette méthode demande des recherches plus approfondies car il existe une ressemblance remarquable quant à la forme générale des pressions dynamiques et statiques, ce qui ne devrait pas être le cas.

Acknowledgements

I would like to thank Professor Laurent Mydlarski for being an outstanding supervisor and for giving me invaluable advice throughout the course of my research. He always found time in his busy schedule for meetings and answered all of my questions in great details. His generous help regarding all aspects of my project was crucial in improving the quality of my work. I have obtained a vast amount of knowledge from him and I am extremely grateful for having been a part of his team.

I would also like to extend my thanks to Alais Hewes, who was always available to answer my questions in the Aerodynamics Laboratory and took time to offer insightful advice. Her assistance was extremely appreciated for the duration of my research. I have learned a great deal from her during my time in the lab.

I am grateful for my family, who constantly provided encouragement throughout my work. I am thankful for my parents' support and belief in me. My brother's support also provided me with motivation for the entire duration of my research.

Finally, I would especially like to thank my grandfather, who inspired me to pursue the sciences. His support has been with me for as long as I can remember, and his words continue to inspire me in life.

Contents

1 INTRODUCTION

1.1 Goals of this Thesis

The goal of this honours thesis project is to enhance the performance of a high-resolution static pressure sensor for turbulence measurements. This will be attempted by way of physical enhancements, as well by optimal digital filtering. An alternate method for indirectly static pressure by making simultaneous pressure and velocity measurements will also be explored. The contents of this thesis will describe the:

1. pressure sensor and its operating principles, and
2. results from flow testing, digital filtering, and simultaneous pressure and velocity measurements.

This thesis begins with a chapter that provides an overview of turbulence from a qualitative point of view. The literature on the topic of static pressure measurements will then be reviewed, followed by the motivation behind the development and enhancement of the pressure sensor. The second chapter introduces the components of the pressure probe and expands on the fundamentals of static pressure measurements. The third chapter presents the results of tests made using the static pressure testing under various flow conditions and analyzes the effects of digital filtering on the signal, followed by the results obtained using simultaneous pressure and velocity measurements. Finally, the thesis concludes with a summary of the results and provides some suggestions for future work on this topic.

1.2 Turbulence - A Brief Overview

1.2.1 Introduction

Turbulence is the most common state of flow in nature and engineering alike. The flow in the earth's boundary layer is turbulent, as is the flow of currents underneath the ocean's surface [1]. The wake of the earth in the solar wind is also a turbulent phenomenon, along with interstellar gas

clouds across the universe. Flow over a golf ball is also made turbulent by the dimples on the ball's surface to delay flow separation. Wings on an aircraft also feature growing turbulent boundary layers. The ubiquitous nature of turbulence gives it relevance in numerous fields and disciplines. The following subsections present an overview of turbulence.

1.2.2 A Qualitative Description of Turbulence

A thorough understanding of turbulence has immediate applications to various fields, such as atmospheric science or aerodynamics. Laminar flows are infrequently encountered in fluid dynamics, and are generally characterized by small densities, small velocities, small dimensions, and/or high viscosities. Further discussion of turbulence, however, is better accompanied by differentiating it from laminar flow. The obvious distinctions between laminar and turbulent flows arise in the form of chaotic and random behaviours of fluid properties associated with the latter. Some of the fundamental characteristics of turbulent flows are summarized below:

- Dissipation - as a result of viscous shear stresses, which perform deformation work, the internal energy of the fluid increases at the cost of a decrease in the kinetic energy. A continuous supply of energy is therefore required in order to compensate for the kinetic energy losses. Any disruption in the energy supply will lead to a rapid decay of the turbulence due to its high rate of dissipation of turbulent kinetic energy.
- Vorticity - high levels of vorticity fluctuations are present due to the rotational nature of turbulent flows. These fluctuations exist in three dimensions and are subject to vortex stretching. Two-dimensional vorticity fluctuations cannot exhibit vortex stretching, which is primarily a feature of three-dimensional turbulent flows.
- Diffusivity - this is the rapid mixing and increased rates of mass, momentum and energy transfer. This property of turbulent flows is of critical importance to engineering applications, as the mixing of momentum can delay boundary layer separation and also increases heat transfer rates in various machines.
- Turbulent flows are flows - since turbulence is a feature of fluid flow as opposed to a fea-

ture of fluids, each turbulent flow exhibits characteristics that are dependent upon initial and boundary conditions. The equations of motion are non-linear and do not have a known general solution, and consequently the study of turbulence is focused on understanding classes or groups of turbulent flows.

While these are some of the key characteristics of turbulent flows, there also exists a notion of an ***energy cascade*** that is crucial in describing the scales of turbulent motion and the distribution of turbulent kinetic energy amongst these scales [2]. Coupled with the ***Kolmogorov hypotheses***, the aforementioned topic serves to provide insight into the smallest scales of turbulent motion, which will be of relevance for the subject matter discussed in this thesis.

In describing the energy cascade, the first important observation is that turbulence is composed of eddies of various sizes. An eddy can be considered to be a turbulent motion that is localized and coherent over a region. For large eddies, their lengthscales and characteristic velocities are comparable to those of the overall flow. At these scales, the Reynolds number (to be discussed later) of the eddies is relatively large, and thus the viscous effects are often negligible.

Large eddies are, however, unstable, and tend to break up into smaller eddies, which in turn break down into smaller eddies still. Energy is transferred from larger eddies to smaller eddies in the process, creating an energy cascade in which energy is continuously transferred to smaller and smaller eddies, until the local Reynolds number of an eddy becomes small enough such that eddies can no longer break down. At this scale, kinetic energy is dissipated through molecular viscosity, and the Reynolds number approaches unity. The scales of the smallest eddies, as well as their dependence in space and/or time are addressed by Kolmogorov's theory, which is a set of three statements, consisting of one postulate and two hypotheses.

Kolmogorov's postulate of local isotropy states that information regarding the geometry of the large scale eddies (corresponding to boundary conditions) is lost as energy is passed down the energy cascade and that the smallest scales become (locally) isotropic. As an immediate consequence, it is inferred that small scale motions of eddies are statistically universal and similar for all

turbulent flows with high Reynolds numbers. Kolmogorov's first hypothesis states that for sufficiently high-Reynolds-number flows, these small scale motions have a universal form and become dependent entirely upon the dissipation rate of turbulent kinetic energy and the kinematic viscosity of the flow. The second Kolmogorov hypothesis further argues that for eddies with scales in between the smallest eddies (dissipative subrange) and the largest eddies, the effects of viscosity are negligible and thus the motions at this scale (so called the *inertial subrange*) are functions of the dissipation rate alone. The statistics in this inertial subrange are then independent of the kinematic viscosity.

1.2.3 A Statistical Description of Turbulence

In the study of turbulence, analysis is often conducted using a statistical approach. It is therefore beneficial to introduce certain parameters and equations that are of relevance in describing turbulence. The primary dimensionless number that is used throughout fluid mechanics is the Reynolds number, which is defined as:

$$Re = \frac{\rho U l}{\mu}, \tag{1}$$

where ρ is the density of the fluid [kg/m^3], U is the fluid's characteristic velocity [m/s], l is the characteristic length of the flow [m], and μ is the fluid's dynamic viscosity [kg/(m $\cdot$ s)]. The Reynolds number represents the ratio of the inertial forces to the viscous forces of a flow.

In general, higher Reynolds numbers are associated with turbulent flows. For the case of external flows, it can be assumed that turbulent flows occur when $Re \gtrapprox 10^5 - 10^6$. As the Reynolds number grows to large values, the viscosity of the flow becomes negligible. Turbulent flows are therefore dominated by inertial forces, which lead to instabilities such as eddies.

It is also beneficial to familiarize oneself with the equations of fluid motion [2]. The first of these equations is the continuity equation, commonly written as:

$$\frac{\partial \rho}{\partial t} + \boldsymbol{\nabla} \cdot (\rho \boldsymbol{U}) = 0. \tag{2}$$

The continuity equation is a statement of conservation of mass.

The second equation is the equation of conservation of momentum, derived from Newton's Second Law. It relates the acceleration of a fluid particle to the to the surface and body forces experienced by the fluid. For an incompressible fluid with constant properties and where the only body force experienced is gravity, one obtains the Navier-Stokes equations:

$$\rho \frac{D\boldsymbol{U}}{Dt} = -\boldsymbol{\nabla} p + \rho \boldsymbol{g} + \mu \nabla^2 \boldsymbol{U}. \tag{3}$$

In summary, the equation states that the acceleration of a particle is related to the pressure and viscous forces within the fluid in addition to the external forces (gravity in this equation). Since this is a partial differential equation, its solution depends upon the specified initial and boundary conditions, which are unique for any given flow. The Navier-Stokes equations in general do not always have closed-form solutions in three-dimensions. Since the Navier-Stokes equations describe the behavior of fluids for countless engineering applications, their solutions are of critical importance to the understanding and modeling of flows. Studies and analysis of these equations often resort to methods of direct measurements in order to approximate and understand the behaviour of turbulence.

It is now advantageous to revisit the Kolmogorov hypotheses and examine them from a quantitative perspective. Given the dissipation rate of kinetic energy (ε) and the kinematic viscosity (ν), the Kolmogorov scales are defined:

$$\eta \equiv (\nu^3/\varepsilon)^{1/4}, \tag{4}$$

$$u_\eta \equiv (\varepsilon\nu)^{1/4}, \text{and} \tag{5}$$

$$\tau_\eta \equiv (\nu/\varepsilon)^{1/2}. \tag{6}$$

These equations describe the length, velocity, and time scales, respectively, of the smallest sized (dissipative) eddies. It should be noted that the Reynolds number describing these micro-

scales is:

$$Re = \frac{\eta u_\eta}{\nu} = 1.$$

In addition to the Kolmogorov scales, the Taylor microscale is also frequently used to describe turbulence. While the Kolmogorov scales represent the smallest scales of eddies responsible for energy dissipation, the Taylor scales do not have a clear physical interpretation. The Taylor microscale can be defined as follows:

$$\lambda = 15\nu \left\langle \left(\frac{\partial u}{\partial x} \right)^2 \right\rangle, \tag{7}$$

which is then used to define a Taylor-scale Reynolds number, often used to quantify the intensity of turbulent flows:

$$R_\lambda = \frac{u' \lambda}{\nu} \ . \tag{8}$$

Here, u' denotes the root-mean-square of the fluctuating component of velocity in the x direction.

1.3 Motivation & Literature Review

Historically, much of the experimental knowledge in turbulence has been accumulated through velocity measurements. Common velocity measurement techniques include hot-wire anemometry, laser Doppler velocimetry, and particle image velocimetry. These measurement techniques have been adopted by turbulence researchers and have been refined over the years. Consequently, velocity measurements have been responsible for the majority of the growth of understanding in the field of turbulence and have also served as the groundwork for existing literature in the field. The vast influence of velocity measurements on advancements in turbulence is, however, strongly contrasted by the scarce literature readily available on pressure measurements.

Further theoretical advancements in pressure-based characterization of turbulence are hindered by the inability to make highly resolved pressure measurements. Although static pressure fluctuations are embedded within the previously introduced equations of fluid motion, they could

not be easily measured using conventional equipment until recently. This is the primary issue that will be further addressed in this thesis, and the research will be guided by literature previously published on this subject.

A high spatial and temporal resolution static pressure probe was previously constructed by Tsuji & Ishihara [3] in 2003 to measure the fluctuating static pressure in a turbulent flow. The authors of the paper recorded static pressure data in the wake of a cylinder with average velocities ranging from $5 \leq U \leq 10$ m/s. The pressure probe utilized a piezoresistive transducer and a standard quarter-inch condenser microphone housed inside a streamlined probe to measure pressure fluctuations in the flow. Results from the measurements were presented in the form of pressure spectra, depicting the intensity of pressure fluctuation as a function of their frequency.

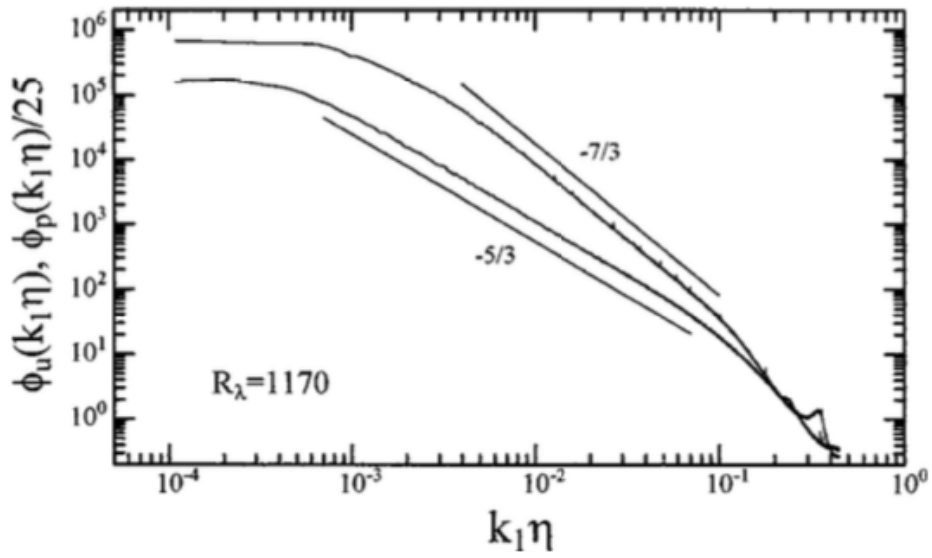

Figure 1: Velocity (bottom curve) and pressure (top curve) spectra normalized by Kolmogorov scales [3].

The pressure measurements were used to study the power-law scaling of pressure spectra in the inertial subrange, which remains a topic of discussion and one for which no definitive conclusions have been drawn. As figure 1 illustrates, the pressure spectrum follows a slope of approximately -7/3 in the scaling region (while the velocity follows a -5/3 slope) on a log-log plot.

This power law can be used to establish and contrast pressure spectra from velocity spectra. Upon studying the variation of the pressure spectra with flow conditions, the authors established that the power-law of -7/3 was observed for $R_\lambda \geq 600$.

The same probe design was also previously utilized to detect three-dimensional vortical structures in a rectangular jet [4]. As pressure fluctuations play an important role in turbulent shear flows, their measurement can be used to analyze turbulence structures and provide deeper insight into the behaviour of vortical structures, which are closely related to pressure fluctuations. The authors measured the phase-average fluctuating pressure over the flow field and were able to observe the interactions of vortices, in addition to their decay into smaller vortices. This work also noted that direct measurements of static pressure fluctuations were very effective in detecting three-dimensional vortical structures.

The validity of the measurement techniques using the aforementioned pressure probe design was investigated in detail in the form of a PhD thesis [5] published in 2014. Simultaneous measurements of velocity and static pressure were taken in the wake of a cylinder to investigate the velocity-pressure correlation. Measurements were taken in the wake of a cylinder as the large-scale vortices shed by the cylinder result in significant velocity-pressure correlation. Effects of the static pressure probe's geometry as it pertains to the interference between the pressure and velocity measurements were also studied by using 10 different pressure probe configurations. Variables in the different configurations included the tube length and diameter.

The study concluded that the interference between the static pressure and velocity probes depended primarily upon the tube diameter of the pressure probe and very weakly upon the length of the tip section. Experimental results were compared and validated against large-eddy simulations. The combination of a hot-wire probe and a static pressure probe was deemed viable in measuring the velocity-pressure correlation, which is a conclusion that will be of relevance further in the thesis.

Inspired by the aforementioned work of Tsuji & Ishihara [3], a static pressure probe was

constructed by a previous student in the Aerodynamics Laboratory to measure static pressure fluctuations in turbulent flows. The constructed probe, however, did not record data with a good signal-to-noise ratio (SNR), and pressure spectra recorded using the probe exhibited high levels of noise in the higher frequency region ($>$ 1kHz). Because more data was required to explain the behaviour of the probe, it remained to be determined whether the poor SNR originated from a lack of a clear signal or from excessive levels of noise in the flow.

To that extent, the goal of this thesis is to enhance the SNR of the pressure probe through physical modifications as well as digital filtering and to replicate the results from the literature. The following sections will outline the operation of the probe as well as the results obtained using the modified designs.

2 EXPERIMENTAL SETUP & APPARATUS

2.1 Static Pressure Probe

To measure fluctuations in static pressure, a pressure probe based on the design used by Tsuji & Ishihara [3] was developed. The static pressure probe consists of a number of parts that together allow the measurement of the static pressure in the flow. The experimental setup was arranged in accordance with descriptions of instrumentation and apparatus that exist in the literature.

2.1.1 Condenser Microphone

The main instrument in the pressure probe assembly is the condenser microphone (PCB model 378A14), which serves as the pressure sensor for all measurements. The model 378A14 is a 1/4" prepolarized pressure field condenser microphone, with a sensitivity of 1.0 mV/Pa [6]. The preamplifier paired with this microphone is the PCB model 426A05 ventless preamplifier. To ensure comparability of results as well as consistency with literature, the microphone was selected in accordance with the model used by Tsuji & Ishihara [3].

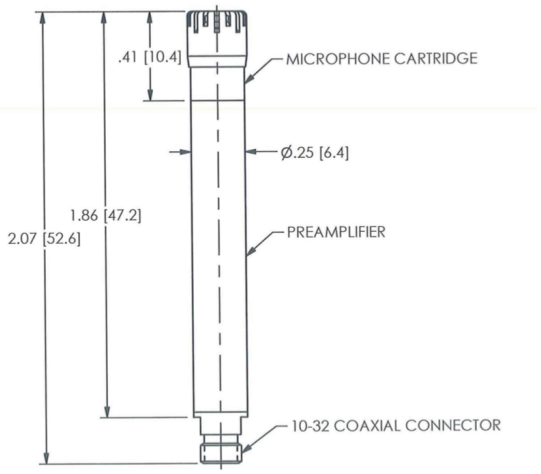

Figure 2: Schematic of the condenser microphone used for data collection in this thesis [6].

Since the operation of the pressure probe is dependent upon the microphone, it is beneficial

to discuss the fundamentals of microphones in further detail. In general, a condenser microphone is an instrument designed to convert pressure oscillations into corresponding voltage oscillations, with the two variables being related through the microphone sensitivity in the following way:

$$Voltage(mV) = Pressure(Pa) \times Sensitivity(mV/Pa) \ . \tag{9}$$

The basic operating principle for a condenser microphone involves the use of a thin metal membrane (diaphragm) arranged in close proximity to a solid metal plate (backplate) [7]. This arrangement results in a variable capacitor that is able to convert the diaphragm's motion into a voltage signal. Charge differential between the diaphragm and the backplate is maintained through voltage application for an externally polarized microphone, while for the case of a prepolarized microphone, the charge is created through the properties of the material itself. Variations in pressure (or sound) result in motion of the diaphragm relative to the backplate, and the resultant change in voltage is proportional to the pressure exerted on the diaphragm.

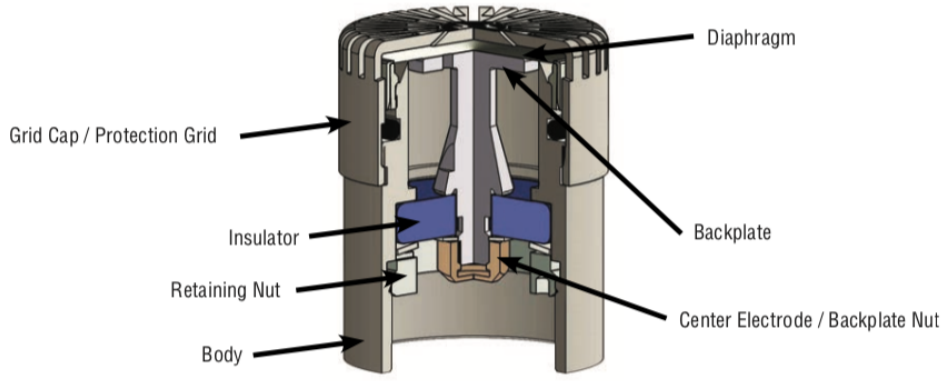

Figure 3: A cross-sectional view of a standard condenser microphone [7].

Another important parameter used to classify a microphone is its response field, which corresponds to the environment under which it is to be operated. In general, there are three types of response fields, each associated with a different acoustic field-type: free-field, random incidence, and pressure-field. A free-field microphone is designed for situations where the sound originates

from a single source directed towards the microphone [8]. These microphones are tuned such that their presence in the acoustic field is accounted for. A random incidence field is one where the sound does not necessarily originate from a single source, but rather the sound travels to the microphone from numerous angles. A random-incidence field microphone should be used in locations with reflective surfaces. The pressure-field microphone is designed for measuring the pressure in front of the diaphragm, and is typically used in an enclosed cavity or is flush mounted in a wall. For the purposes of static pressure measurements, where the microphone is to be mounted inside of a cavity, a pressure-field microphone is optimal.

(a) Free-field microphone (b) Random-incidence microphone (c) Pressure-field microphone

Figure 4: A microphone in different types of acoustic fields [8].

2.1.2 Probe

The static pressure probe used consists of a thin-walled tube with a circular cone as a tip. Four 0.4 mm diameter holes were laser-drilled around the circumference of the tube separated by 90^o. These holes allow the static pressure of the flow to be captured and travel through the tube to the cavity. The end of the probe has a flared part that houses the condenser microphone. A cavity has been built into the probe such that it acts as a chamber in front of the microphone and allows the pressure of the air to push against the diaphragm.

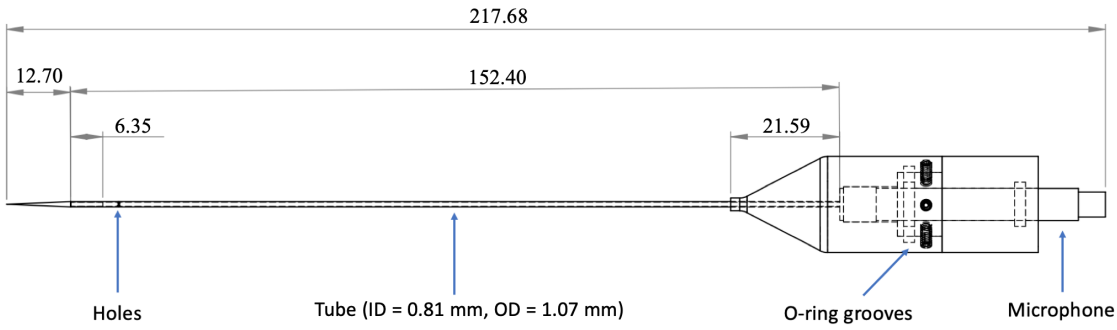

Figure 5: Schematic depicting the dimensions (in mm) of the static pressure probe.

Due to the challenges of machining small parts present in this design, aluminum was selected as the construction material, while stainless steel was used only for the tube. The size and shape of the probe base were significantly influenced by the fact that the probe had to be minimally intrusive when introduced into the flow while still being able to properly house the microphone. Grooves for O-rings were carved into the base in order to prevent air leakage, as this would alter the static pressure in the cavity of the probe.

The dimensions of the tube and cavity result in a Helmholtz resonator frequency for the probe. Helmholtz resonance is a phenomenon that can be observed due to the effects of air resonance in a cavity. This phenomenon can be used to explain the frequencies or pitches of various musical instruments or other geometries (e.g. blowing air across the top of an empty bottle). The formulation for the resonator frequency is as follows:

$$f = \frac{c}{2\pi}\sqrt{\frac{S}{l \cdot V}}, \tag{10}$$

where, f is the Helmholtz resonator frequency, c is the speed of sound in the medium, S is the cross-sectional area of the tube, l is the length of the tube, and V is the volume of the cavity.

Given the dimensions and geometry of the static pressure probe, $f = 666$ Hz. Therefore, one would expect to see a spike or disturbances in the spectrum at this frequency, and altering the resonator frequency appropriately can shift the disturbance to the desired frequency, which can be

advantageous for analysis.

2.2 Signal Conditioner

The condenser microphone requires a constant current power source to ensure proper functionality. This constant current power is provided via the model PCB 480E09 signal conditioner. This battery powered unit consists of current-regulation diode and a capacitor for decoupling the signal (thus removing the bias voltage), and offers amplification factors (gains) of 1, 10, and 100. Using two BNC cables, the signal conditioner can be connected to the microphone and to the data acquisition system.

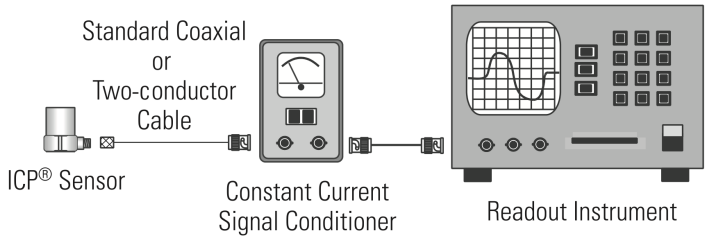

Figure 6: A typical configuration involving a signal conditioner and sensor [9].

The gain provided by the signal conditioner is:

$$Gain = \frac{V_{out}}{V_{in}}. \tag{11}$$

2.3 Data Acquisition System

Measurements with the pressure probe were taken in a wooden wind tunnel for internal flow conditions, and in a planar jet at the exit of a high-aspect-ratio channel for external flow conditions. For all measurements, the condenser microphone was connected via BNC cables to signal conditioner, which itself was connected to the connector block (National Instruments model BNC-2110) via the signal conditioner. The gain was applied to the signal through the amplification setting provided

on the conditioner. The signal was then low-pass and high-pass filtered through a band-pass filter (Krohn-Hite model 3384). The low pass frequency was set by examining the spectrum and setting it such that the minimum point of the spectrum was properly recorded. Any signal following the minimum was deemed noise and filtered out. The high-pass frequency was set to 0.1 Hz for all measurements.

Figure 7: Schematic of the experimental setup.

The data acquisition card used was the PCI-6036E with a range of ± 10 V. LabVIEW programs were then used to monitor the signal and record the data, with the sampling rate set to twice the low-pass frequency in order to avoid aliasing effects. For most measurements, 200 blocks of data were collected with each block consisting of 16,384 samples. Unless otherwise specified, a sampling frequency of 20 kHz was used when recording spectra.

Analysis of the data was conducted through FORTRAN 90 codes that allow for extraction of statistical as well as spectral representations of input data. The power spectrum of the fluctuating pressure measurements is calculated by performing a Fourier transform on the time-series signal and plotting the power spectral density against the corresponding frequencies. Smoothing and refinement of the spectra is also achieved by using window functions embedded within the code.

3 RESULTS

3.1 Physical Enhancements

In an attempt to improve the SNR of the static pressure measurements, modifications and physical enhancements were made to the pressure probe. These modifications and enhancements included varying the signal conditioning, tube length of the probe, flow conditions, vibration reduction, and increasing the pressure signal by increasing the flow speed.

The following subsections discuss the effects of each modification to the measured data, and conclude whether there exists an optimal condition or value for each variable such that improvements in pressure spectra are observed. Effects of each variable on the quality of the spectra will be studied by ensuring that other variables are maintained constant. All measurements consisted of 200 blocks of data, with each block consisting of 16,384 samples. The high pass frequency was set to 0.1 Hz and the low pass frequency was determined by examining the instantaneous spectrum such that all noise beyond the minimum point of the spectrum was filtered. The sampling frequency was set to twice the low pass frequency to avoid aliasing effects.

3.1.1 Signal Conditioning

The first variable considered in the experimental setup was the gain provided by the signal conditioner. The gain setting allows for amplification of the signal. Taking this into account, pressure spectra for identical (internal) flow conditions were examined where the only parameter being altered was the signal conditioner's gain setting. Gain settings of 1, 10, and 100 were used to record data to examine their effects on the SNR of the probe and to determine whether there was an optimal setting for which improvements in spectra were observed.

Analysis of test results showed that improvements in the SNR were observed with larger gains, as can be observed in figure 8. This result was in good agreement with expectations as the gain in general increases the SNR by amplifying the signal. Therefore, low energy fluctuations were better resolved using the highest gain setting. The gain setting of 100 was selected for signal

conditioning for all further measurements. Nevertheless, figure 8 clearly exhibits noise (spikes) in the inertial subrange of the spectra, even at the highest gain. Thus other means will be attempted to improve the SNR of the static pressure probe.

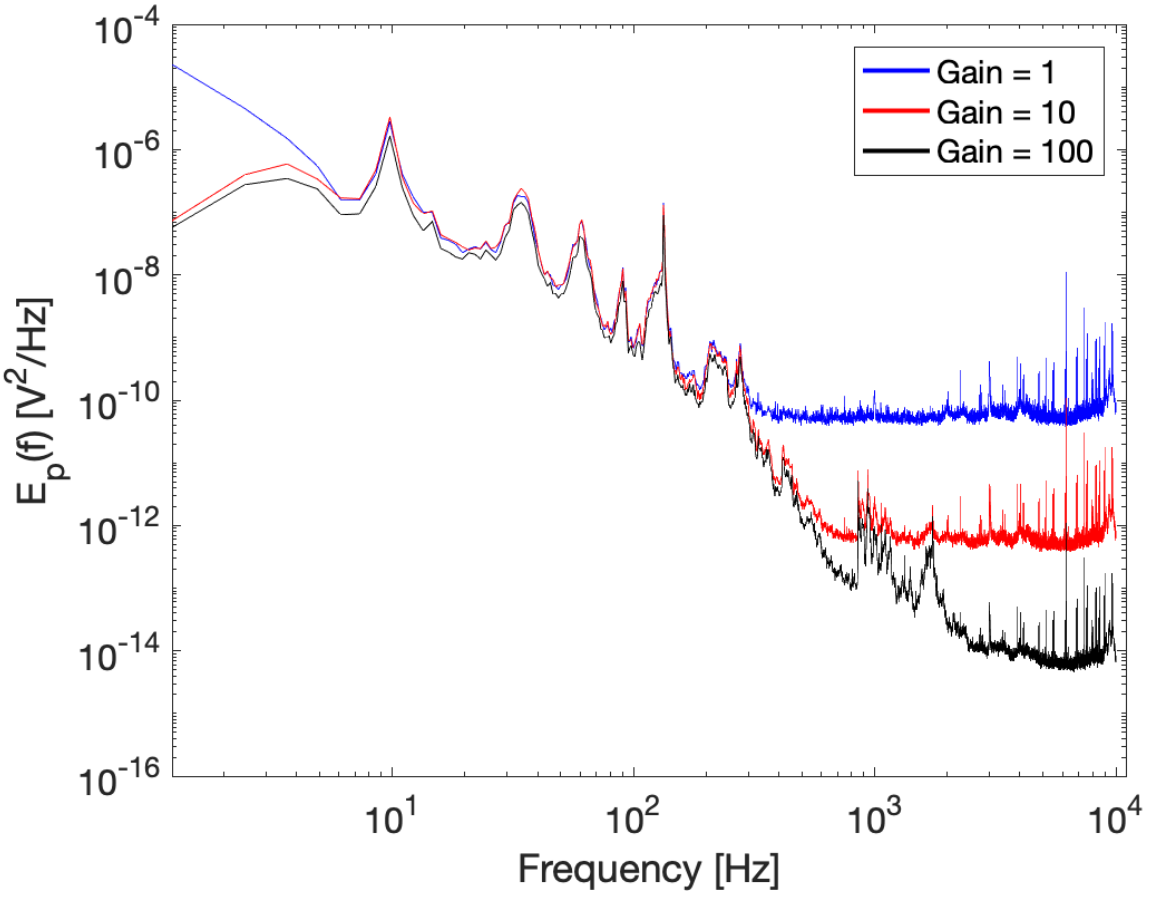

Figure 8: Effects of the gain setting on the pressure spectra.

3.1.2 Effect of Tube Length

The tube length for the pressure probe was selected as 140 mm for the probe's initial design by a previous student. Subsequent literature review on the topic, however, revealed that the first design for the static-pressure probe proposed by Shirahama & Toyoda [10] in 1993 used a tube with a length of 40 mm.

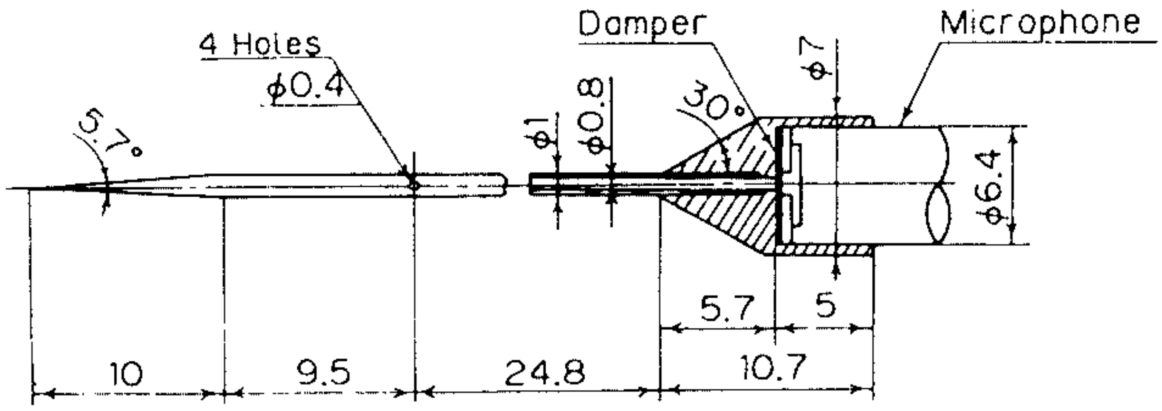

Figure 9: Schematic of the static pressure probe designed by Shirahama & Toyoda [10] with all dimensions in millimeters.

As figure 9 illustrates, the total length of the tube (not including the conical tip) was $l = 9.5 + 24.8 + 5.7 = 40$ mm. The implementation of a new tube length would also alter the effective Helmholtz frequency given by equation (10). The construction of the new, shorter tube was carried out using the same stock tube dimensions illustrated in figure 5 so as to maintain all other parameters constant. Varying the value for l in the equation while maintaining the cavity volume and the tube cross-sectional area constant resulted in a new calculated Helmholtz frequency of $f = 1259$ Hz.

As the new tube length implemented was 100 mm shorter than the previously used tube, the effects of tube length on the signal-to-noise ratio could be analyzed by recording data in identical conditions while replacing the longer tube with the shorter one between tests. The tube length was thought to be an essential element of the design as it dictated the extent of the tube's oscillations and vibrations under higher speed flow conditions. A shorter tube length would theoretically be more rigid than a longer tube made from the same material, and therefore might result in an improved SNR, in addition to having a larger Helmholtz frequency.

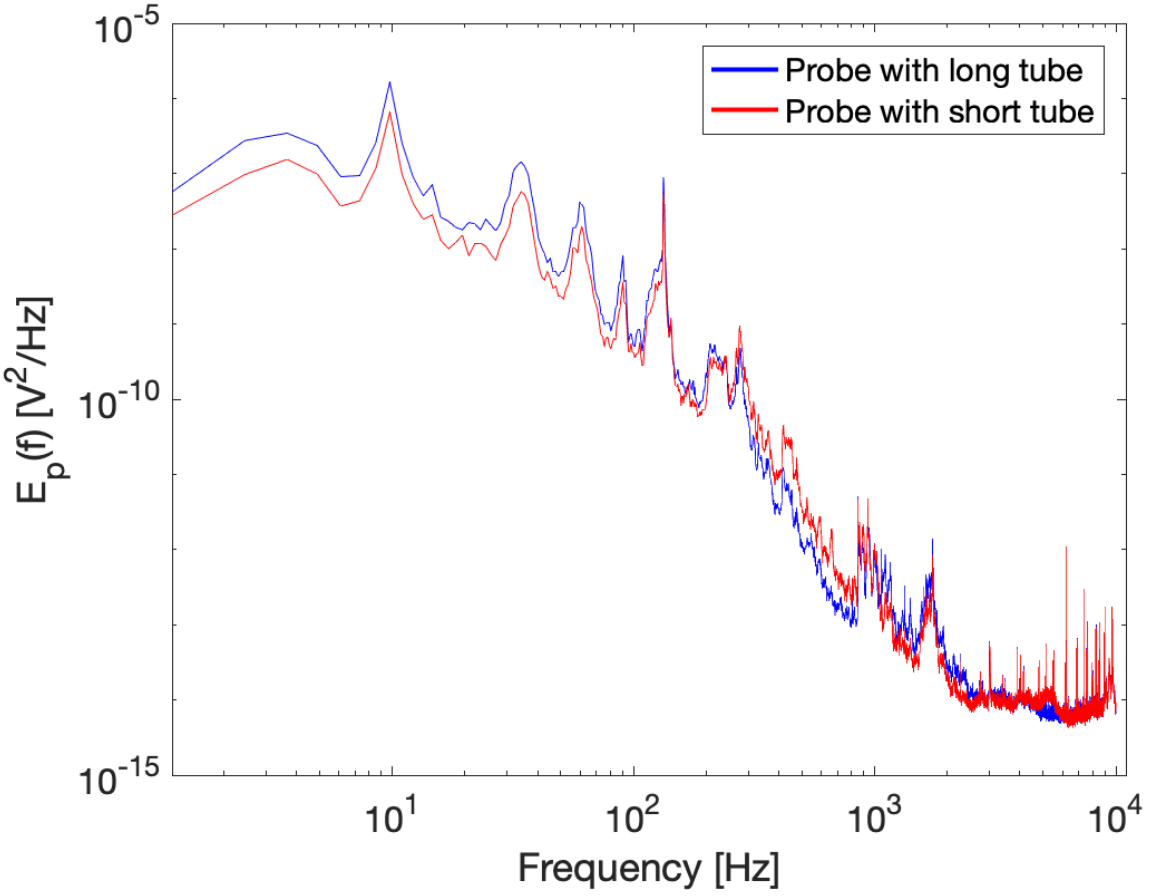

Figure 10: Effect of the tube length on the pressure spectra.

The effects of the tube length on the recorded pressure spectra (in internal flow) are depicted in figure 10. In general, minor differences were observed between spectra recorded by the two tube lengths and any variations in the SNR were considered insignificant. Given the minor effect of the tube length, the longer tube was selected to record future measurements for consistency with prior data collection.

3.1.3 Internal & External Flow

Measurements made with microphones in internal flow conditions are easily contaminated by the propagating acoustic fluctuations generated by the facility which mask the pressure fluctuation

signal originating from turbulence [11], which can also be reflected off the walls in an internal flow. Moreover, the signal can further be contaminated by the vibrations induced in the sensor by the wall to which the sensor is attached. Even in the case of quiet wind tunnels, the measurements can still be polluted by acoustic wave propagation within the tunnel.

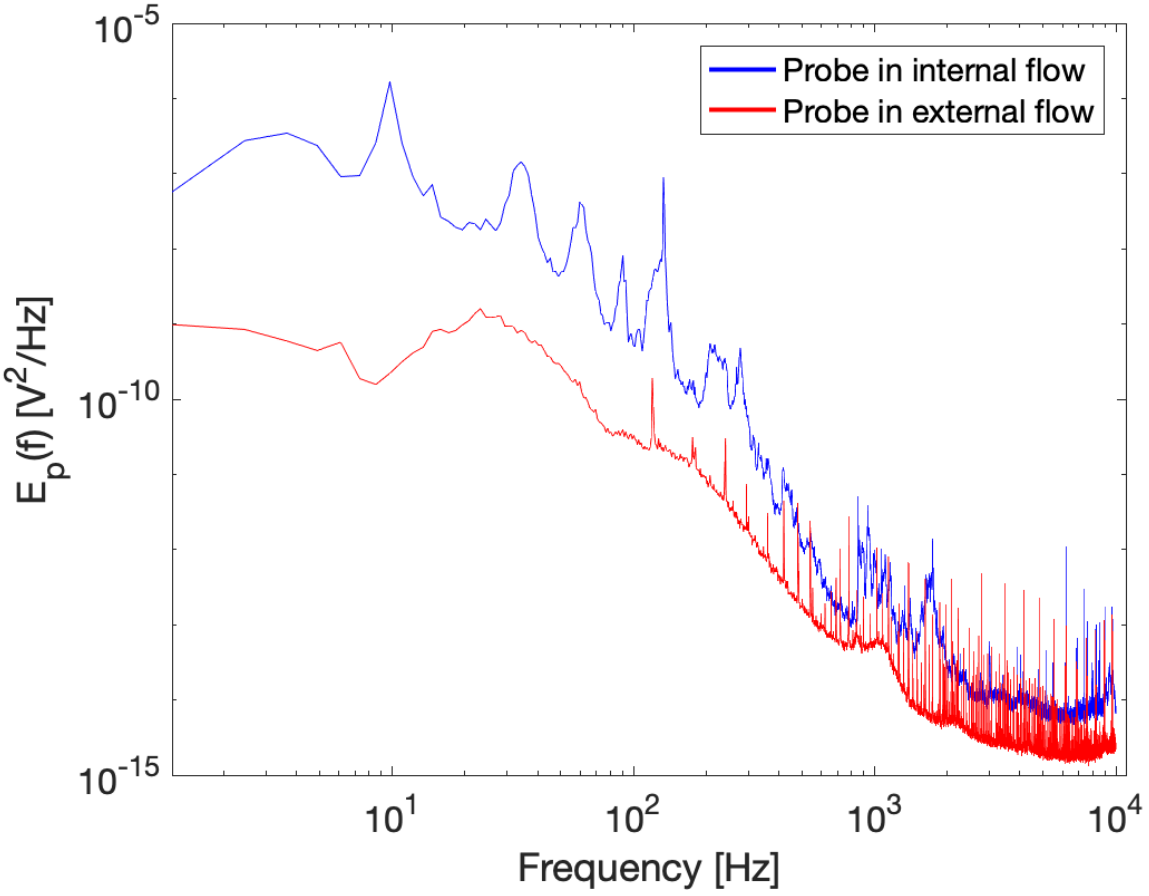

Figure 11: Effects of flow conditions on the pressure spectra.

As all measurements up to this point were recorded inside a wooden wind tunnel, the sensor was prone to contamination from the aforementioned sources of noise. The sensor was especially affected by the wall vibrations as it was inserted into the flow through an elbow attached to the tunnel wall. As an attempt to increase the SNR, the pressure probe was moved to a planar jet, created at the exit of a high-aspect ratio channel, where it would be free from internal flow noise

contamination.

As shown in Figure 11, improvements in the quality of the static pressure spectrum were observed when moving from internal flow to external flow conditions. Less noise was observed for measurements taken in the external flow for the entirety of the frequency domain. This could primarily be attributed to the low-frequency disturbances generated by the wind tunnel which propagate inside the tunnel test section. The vibrations resulting from the tunnel's walls were also eliminated, and consequently the SNR experienced significant improvements when compared to internal flow conditions.

Subsequent data collection was conducted at the exit of the high-aspect ratio channel to prevent contamination resulting from non-ideal internal flow conditions.

3.1.4 Vibration Reduction

The notion of signal contamination as a result of the sensor's own vibrations was introduced and discussed in the previous section. Relocation of the pressure probe from internal flow conditions to external flow conditions improved the response of the probe for the majority of the frequency range. Residual contamination resulting from the probe's vibrations as a result of the passing turbulent flow could still, however, be observed. While the visible magnitude of these oscillations was marginally smaller than those resulting from the tunnel's wall vibrations, these oscillations were still contributing to the pollution of data.

Damping of the residual sensor vibrations was achieved by construction of a new base with a shorter rod length connecting to the probe assembly. Previous experimental setups in internal flows relied upon securing the probe using a longer rod so it could be inserted into the center of the tunnel. Since the apparatus was moved to external flow after considering the results from the previous section, a longer rod was no longer required. The length of the rod connecting the probe to the base was shortened from 50 cm to 10 cm to reduce the swaying of the probe assembly in the flow.

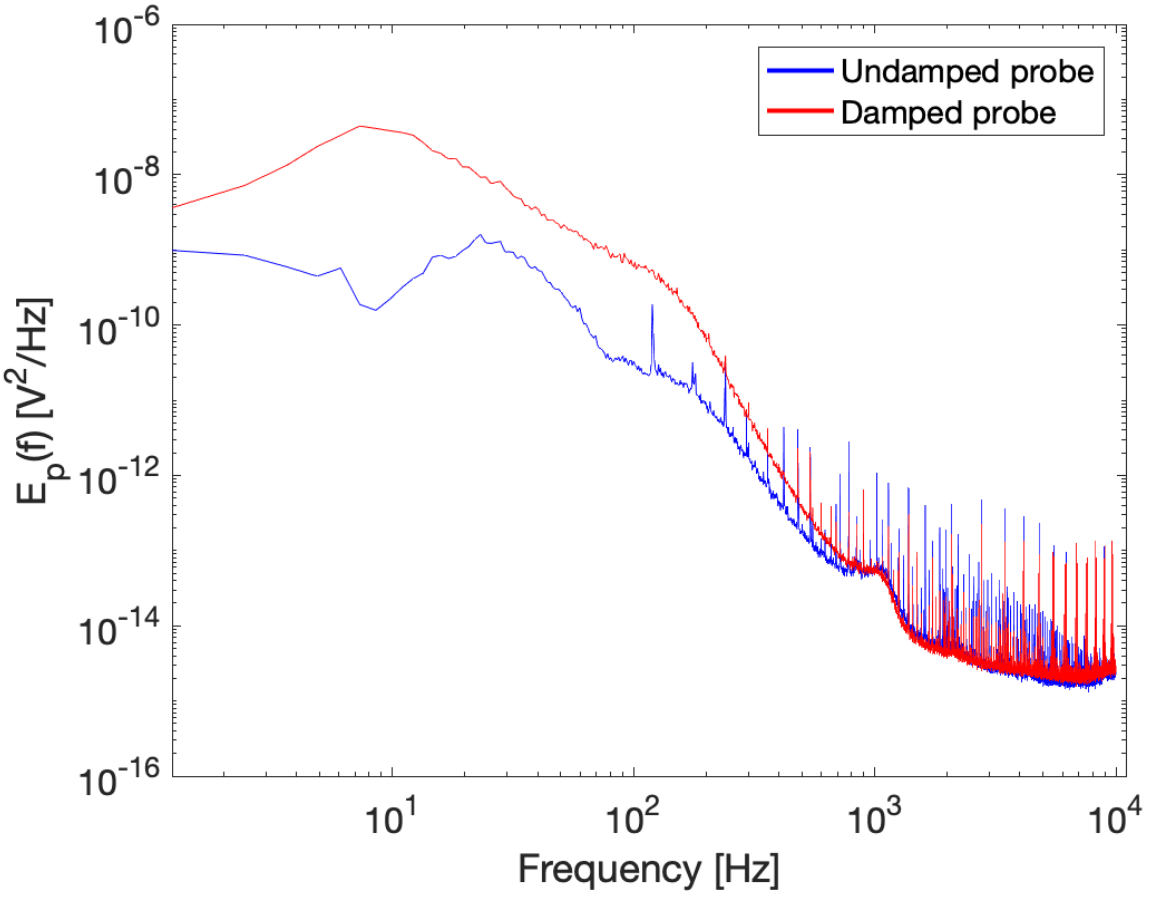

Figure 12: Effects of vibration damping on the pressure spectra.

As observed in figure 12, the reduction of the probe's vibrations resulted in improved SNR, especially in the inertial sub-range. The remaining noise induced spikes in the dissipation region were now observed to be less frequent and occurred at lower amplitudes than those previously observed in the undamped probe scenario. Overall, fewer vibrations were observed in the probe assembly, and consequently the shorter rod and new base were selected as permanent features in the experimental setup.

3.1.5 Increasing the Turbulence Signal

In the previous subsections, the SNR of the probe was increased by reducing the noise encountered by the probe. Alternatively, the SNR could also be increased by increasing the signal itself. This effect was implemented by increasing the fan speed of the channel, resulting in higher flow velocities. The effects of higher fan speeds on the measured spectra were then studied by maintaining other parameters constant.

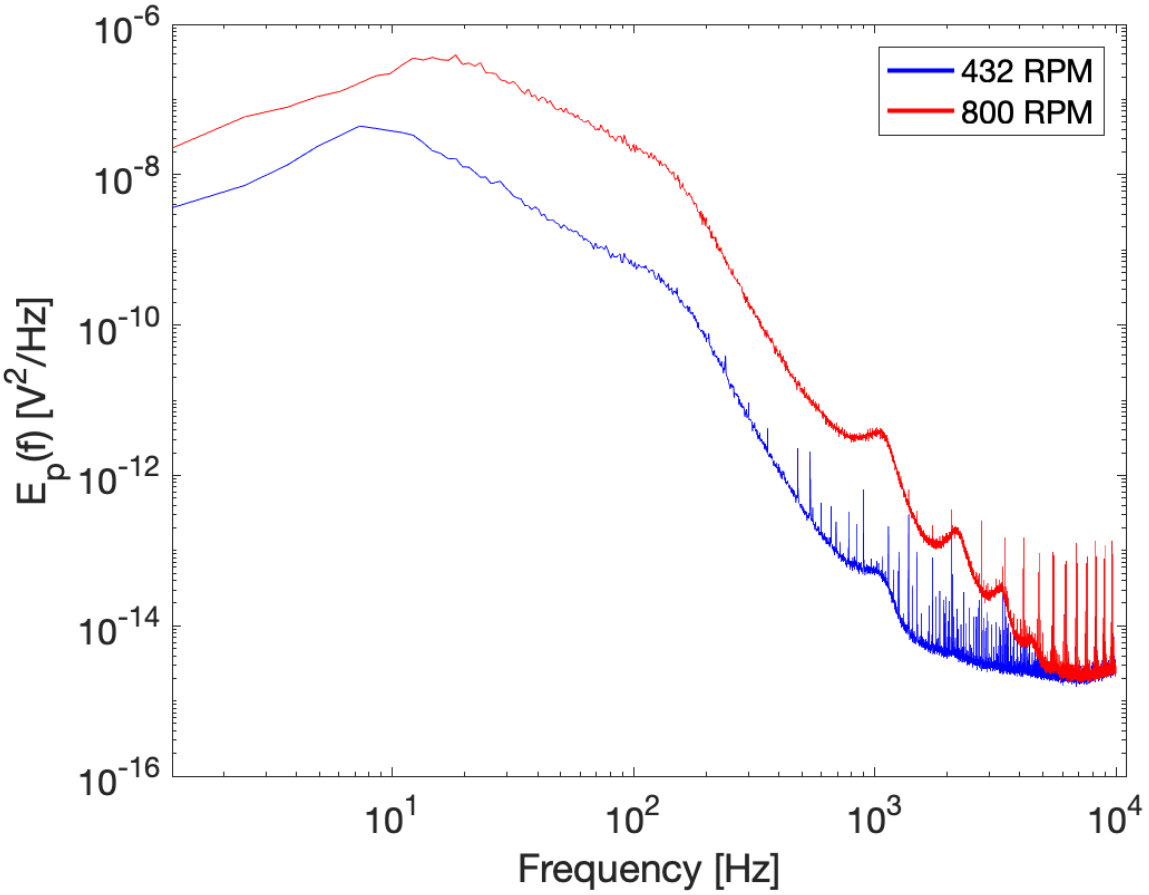

Figure 13: Effects of increased signal levels on the pressure spectra.

Pressure spectra were recorded with fan speeds of 432 and 800 RPM at the exit of the channel. Examination of the recorded data showed, in general, that the quality of the spectra improved

with increasing fan speeds. Spectra recorded with a fan speed of 800 RPM exhibited noise spikes commencing at frequencies of 2kHz as opposed to 450 Hz as previously measured for fan speeds of 432 RPM. Spikes observed in the high frequency domain for 800 RPM also became less frequent when compared to measurements taken in 432 RPM. However, other broadband spikes became visible at the 800 RPM tunnel speed. The source of these spikes requires further investigation.

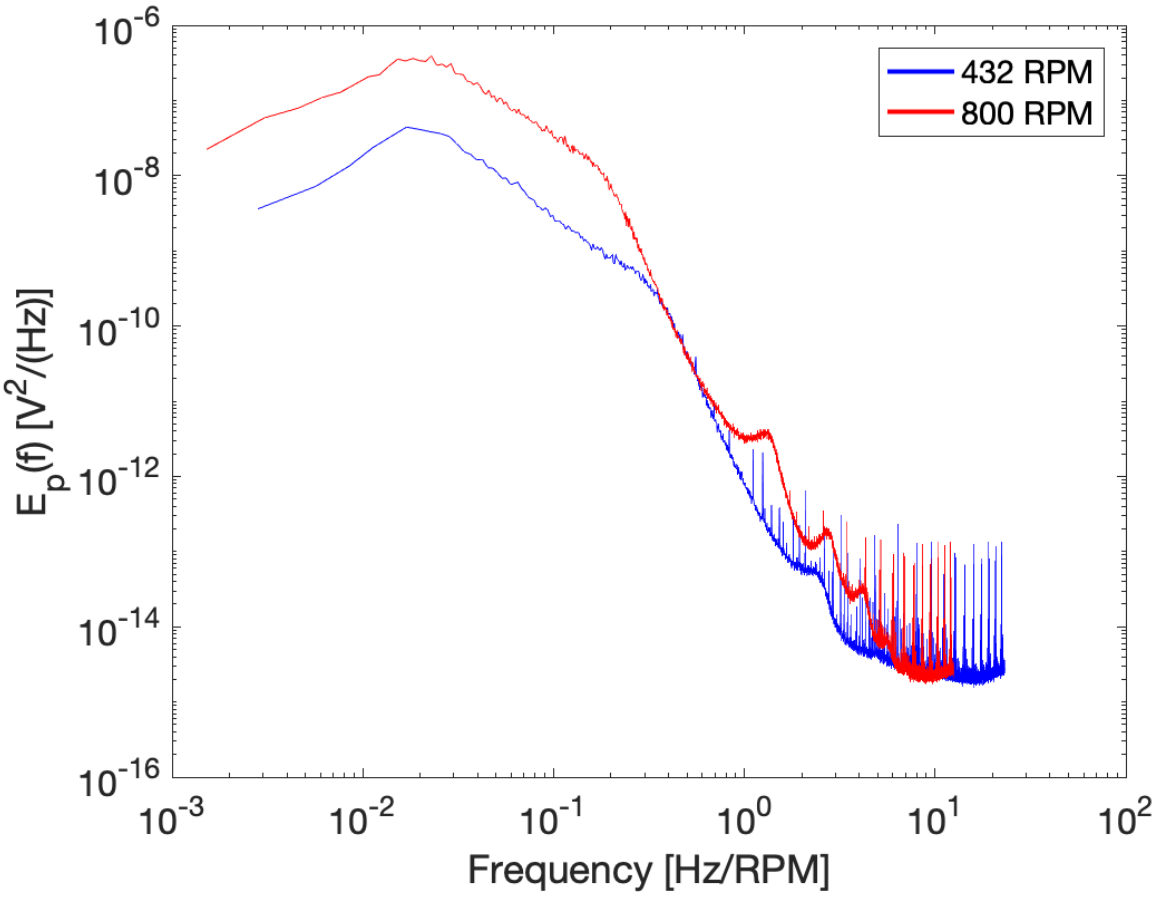

Figure 14: Pressure spectra plotted against the frequency normalized by the respective fan speeds.

Upon further examination of the shape of the recorded spectra, the peaks in the graph appeared to shift to higher frequencies for increasing fan speeds. The suspected source of the peak was the pitch of the operating fan speed of the channel. Normalization of the spectra by their respective fan speeds resulted in a collapse of the spectral peaks, indicating that the fan speed was,

in fact, the source of the displaced peaks observed in the spectra.

3.2 Digital Filtering

3.2.1 Background

In an attempt to further improve the SNR of the pressure probe beyond physical enhancements, a form of optimal digital filtering was applied to the recorded data. This form of optimal filtering was proposed by Naguib et. al [12] in 1996, in which they acknowledged that pressure measurements are often contaminated by sources of noise in the measurement facility or by the probe itself. These factors usually include acoustic noise from the fan/blower, as well as tunnel unsteadiness. The pressure probe itself maybe corrupted by vibrations caused as a result of not isolating it from the measurement facility. These factors combined consequently lead to the fluctuation signal being contaminated by the noise.

Optimal-filtering methods pose an advantage over conventional, subtraction based filtering techniques in the sense that the former allow for the extraction of filtered pressure *time-series*. While subtraction-based techniques are effective at filtering turbulent statistical data, they have proven to be impractical in obtaining noise-cancelled pressure time-series. In addition, optimal-filtering results in losses of energy of turbulent motion at low frequencies due to noise cancellation that is an order of magnitude smaller than losses resulting from subtraction schemes.

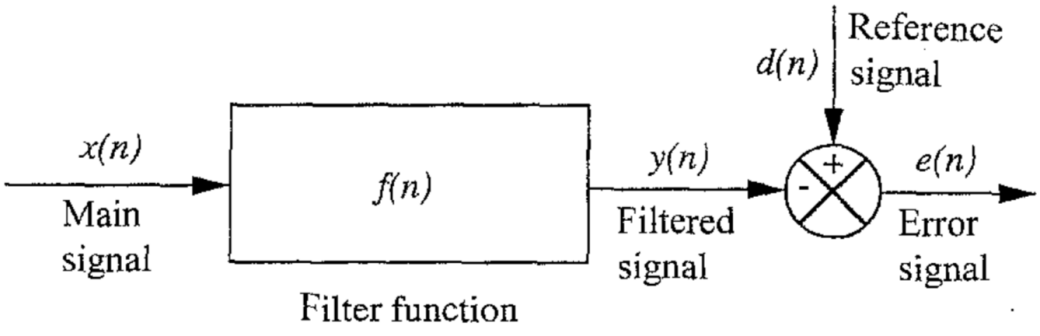

Figure 15: Filter function for a generalized optimal filter [12].

The premise for the proposed optimal filtering technique involves finding a set of filter coefficients $f(n)$ such that a main signal (time-series), $x(n)$, can be passed through the filter and be transformed into a signal that is similar to a reference time signal, $d(n)$. Here $n = 0, 1, ..., L-1$, where L is the number of data points in the main signal. Upon subtraction of the filtered signal, $y(n)$, from the reference signal, $d(n)$, one obtains an error signal, $e(n)$, for which the expectation of its square is minimized by the filter coefficients.

With respect to applications of pressure measurements, $x(n)$ and $d(n)$ are pressure time-series signals measured at identical streamwise locations in the flow separated by a distance δ in the spanwise direction. The value for δ should be large enough such that the turbulence signals measured at the two points are uncorrelated. The noise signals measured at both of these locations, however, should be similar due to their two-dimensional nature. Thus, by extracting the correlated part of the two time-series, one can obtain the undesired noise signal, $y(n)$, embedded in the recorded data. Subsequent subtraction of $y(n)$ from $d(n)$ gives the filtered turbulence signal, $e(n)$, which has been separated from the contaminated noise.

3.2.2 Application

Application of the optimal-filter first requires solving for a set of filter coefficients $f(n)$ for $n = 0, 1, ..., L-1$ that serve as the filter function. This leads to a set of L linear algebraic equations

with L unknown filter coefficients. A matrix equation can then be setup and expressed in the form:

$$\begin{bmatrix} r(0) & r(1) & . & . & . & . & . & r(L-1) \\ r(1) & r(0) & r(1) & . & . & . & . & . \\ r(2) & r(1) & r(0) & r(1) & & & & . \\ . & & r(1) & . & . & & & . \\ . & & & . & . & . & & . \\ . & & & & . & . & . & . \\ . & & & & & . & . & r(1) \\ r(L-1) & . & . & . & . & . & r(1) & r(0) \end{bmatrix} \times \begin{bmatrix} f(0) \\ f(1) \\ . \\ . \\ \\ . \\ . \\ f(L-1) \end{bmatrix} = \begin{bmatrix} g(0) \\ g(1) \\ . \\ . \\ \\ . \\ . \\ g(L-1) \end{bmatrix}, \quad (12)$$

where $r(i)$ is the auto-correlation of $x(n)$ evaluated with a delay of i samples, and $g(i)$ is the cross-correlation between $x(n)$ and $d(n)$ with $x(n)$ being delayed by i samples. Equation (12) is a linear equation of the form $R\mathbf{f} = \mathbf{g}$ for which the solution is concisely given as $\mathbf{f} = R^{-1}\mathbf{g}$, where $\mathbf{f}$, R, and $\mathbf{g}$ are the filter coefficients vector, auto-correlation matrix, and the cross-correlation vector, respectively. Calculation of the auto-correlation matrix, R, is straight-forward and requires finding the auto-correlation values for $x(n)$ which are given by the auto-correlation function expressed in the normalized form as [2]:

$$r(i) = \frac{\langle x(n)x(n+i)\rangle}{\langle x(n)^2\rangle}. \quad (13)$$

In general, the auto-correlation function describes how a function is correlated with itself when the function is evaluated with a time delay of i samples. For $i = 0$ corresponding to a delay of 0 samples, the function will be perfectly correlated with itself (i.e. $r(0) = 1$). For values of $i > 0$, the value for the auto-correlation will be $r(i > 0) \leq 1$. It suffices to assume that for the

generalized case one might expect the auto-correlation of a function to decrease as the delay is increased.

The cross-correlation vector, $\mathbf{g}$, is similarly found by calculating the cross-correlation between $x(n)$ and $d(n)$, which in its normalized form is:

$$g(i) = \frac{\langle d(n)x(n+i)\rangle}{[\langle x(n)^2\rangle\langle d(n)^2\rangle]^{1/2}}, \tag{14}$$

where $g(i)$ measures how correlated the function $d(n)$ is with $x(n)$ when the function $x(n)$ is delayed by i samples. Now that all required inputs for equation 12 have been formally defined, the set of filter coefficients $\mathbf{f}$ can computed and applied to obtain the filtered signal $y(n)$. Assuming a casual Finite Impulse Response (FIR), filtering is achieved by convoluting the filter coefficients with the main signal [13] in the following way:

$$y(n) = \sum_{k=0}^{N} f(k)x(n-k). \tag{15}$$

3.2.3 Filtered Signal

Figure 16 depicts a pressure spectra before and after applying the optimal digital filter.

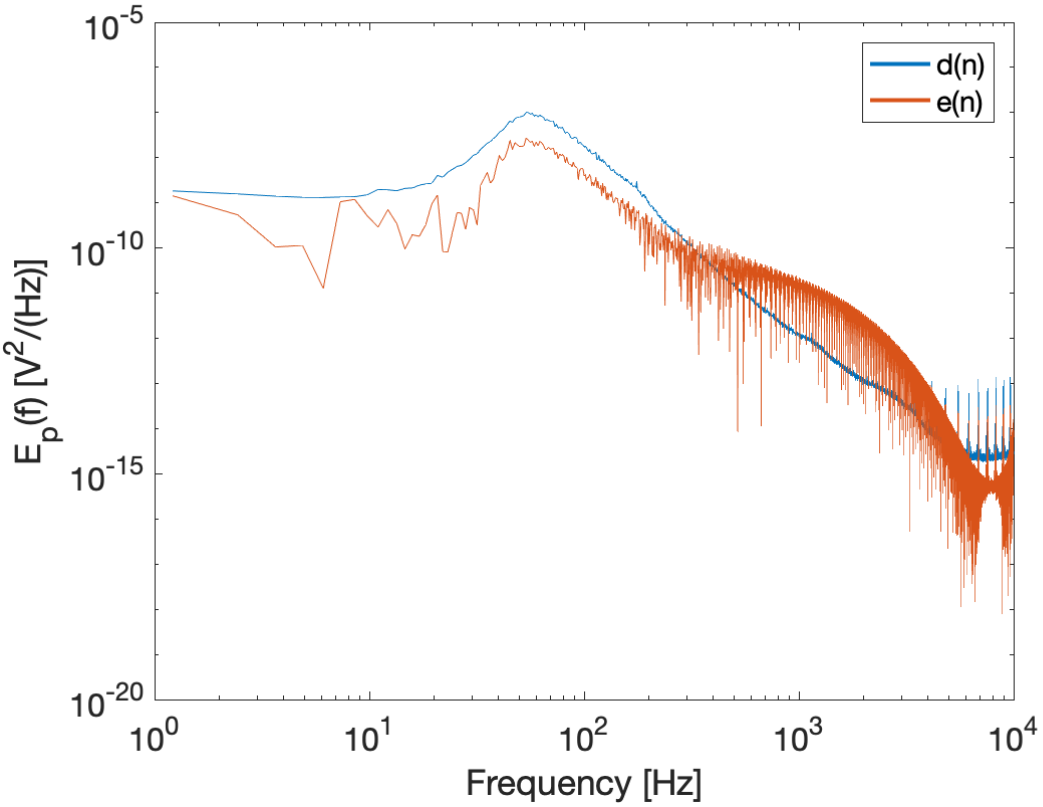

Figure 16: Effects of the filtering the recorded pressure spectra.

Application of the optimal filter to the acquired data did not yield substantially improved results. As figure 16 depicts, the spectral peak in the signal $d(n)$ was unable to be eliminated through the application of this filter, and overall improvements in the quality were not observed. While several reasons may have contributed to the failure of this method, the most relevant in this scenario is perhaps the fact that the noise contamination measured at the two locations was not very well correlated.

Better results may be expected from applications of this method where the noise at two locations is known to be very well correlated. Factors that would cause a poor correlation could be asymmetry of noise distribution about the center line of the channel, unaccounted facility noise contamination, and variation in the noise levels at the two locations.

3.3 Simultaneous Pressure & Velocity Measurements

The results presented thus far in this honours thesis relied upon direct measurement of static-pressure via the static-pressure probe. In this section, an alternate method for obtaining the static-pressure in a flow will be explored. Although the focus of this section is not the improvement of the SNR of the pressure probe, emphasis is still placed upon obtaining high-resolution static-pressure data.

The underlying principles for this method are a direct application of the decomposition of the total (stagnation) pressure such that:

$$P_{total} = P_{static} + P_{dynamic} \, . \tag{16}$$

Furthermore, it is also known that

$$P_{dynamic} = \frac{\rho U^2}{2}.$$

Rearranging equation (16) then yields

$$P_{static} = P_{total} - \frac{\rho U^2}{2}. \tag{17}$$

It becomes evident from equation (17) that the static pressure is dependent upon the total pressure and the velocity of the flow. If the terms on the right hand side of the equation can be measured, then the static pressure of the flow can be deduced. The total pressure can be measured by using the condenser microphone that has been used thus far as the primary component of the probe. Once separated from the probe assembly and inserted into the flow by itself, the voltage difference experienced by the microphone will reflect the magnitude of the *total* pressure fluctuation, since the remainder of the probe assembly was designed to only measure static pressure fluctuations.

Assuming incompressible flow, the only remaining variable in equation (17) remains to be the

flow velocity U. This component can be easily measured by using hot-wire anemometry, which is a well established, high-resolution technique for measuring velocities. Hot-wire anemometry involves heating a very thin wire by passing a current through it. When this wire is placed in a flow, the passing air cools it down and a voltage difference is produced as a result of the wire's changing resistive properties. Through application of convective heat transfer principles, a relationship between the voltage drop across the wire(which is related to the anemometer output voltage) and the flow velocity is derived in the form:

$$V^2 = AU^B + C. \tag{18}$$

In equation (18), A,B, and C are constants that are obtained by calibrating the hot-wire, and V and U are the anemometer voltage and flow velocity, respectively. Using a jet with known velocities at the exit, the anemometer voltage can be related to the jet exit velocities and a non-linear least-squares curve can be fit to the data to obtain the values for the calibration constants.

The experimental setup depicted in figure 17 consisted of placing the condenser microphone next to a hot-wire probe at the exit of the channel. To mitigate spatial effects, the distance between the two probes should be minimized, but not to the extent where interference effects between the two instruments become dominant. The optimal separation distance between the probes was specified by Naka & Obi [14] as $0.5D$, where D is the diameter of the total pressure probe. For the setup with the microphone, this distance was appropriately set to 3.2 mm. The low-pass frequency for each instrument was determined independently based on the instantaneous spectrum. The sampling frequency used for both instruments was set to 12,800 Hz to ensure compatibility of the pressure and velocity data.

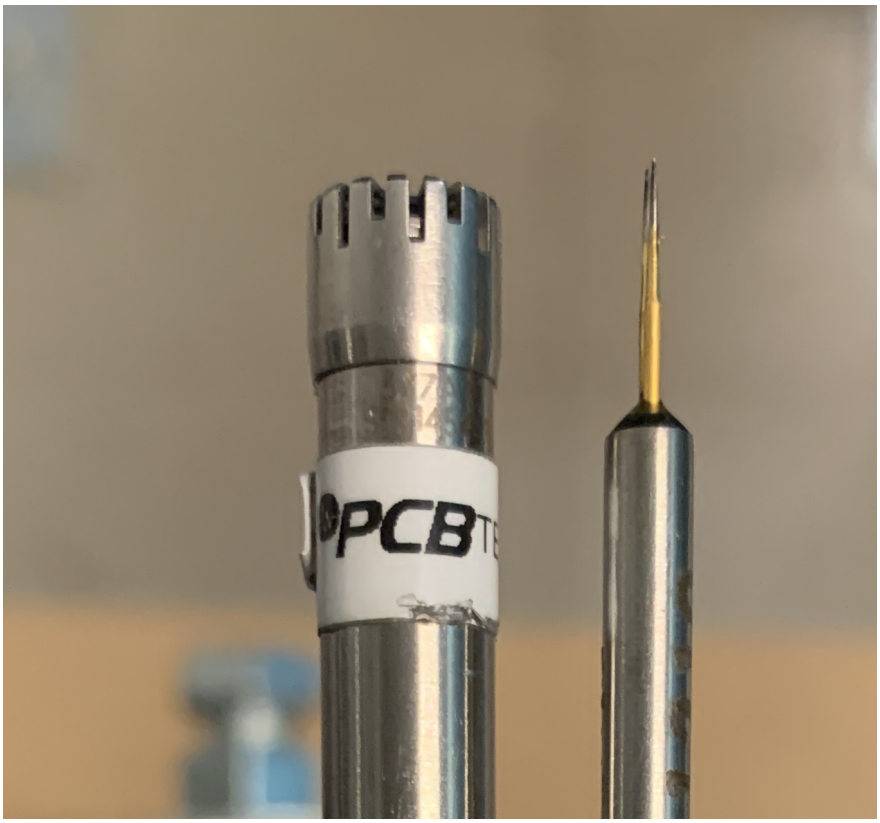

Figure 17: Combination of a condenser microphone with a hot-wire probe.

Once the velocity and total pressure were recorded, the static pressure was calculated by using the following equation [14]:

$$p = p_t - \frac{\rho}{2}(2Uu + u^2 - \overline{u^2}), \tag{19}$$

which is derived from equation (17) by applying a Reynolds decomposition. Upper and lower case-values in the equation represent mean and fluctuating components respectively, while the overbar denotes time averaging.

3.3.1 Results from Indirect Static Pressure Measurement

Plotted in figure 18 are the spectra for total, dynamic, and static pressures. For frequencies between 10 and 1000 Hz, the spectra for all pressure components are easily distinguishable. Once the total pressure begins to drift further away from the dynamic pressure for frequencies beyond 1 kHz, however, the distinction between the static and dynamic pressures becomes less clear.

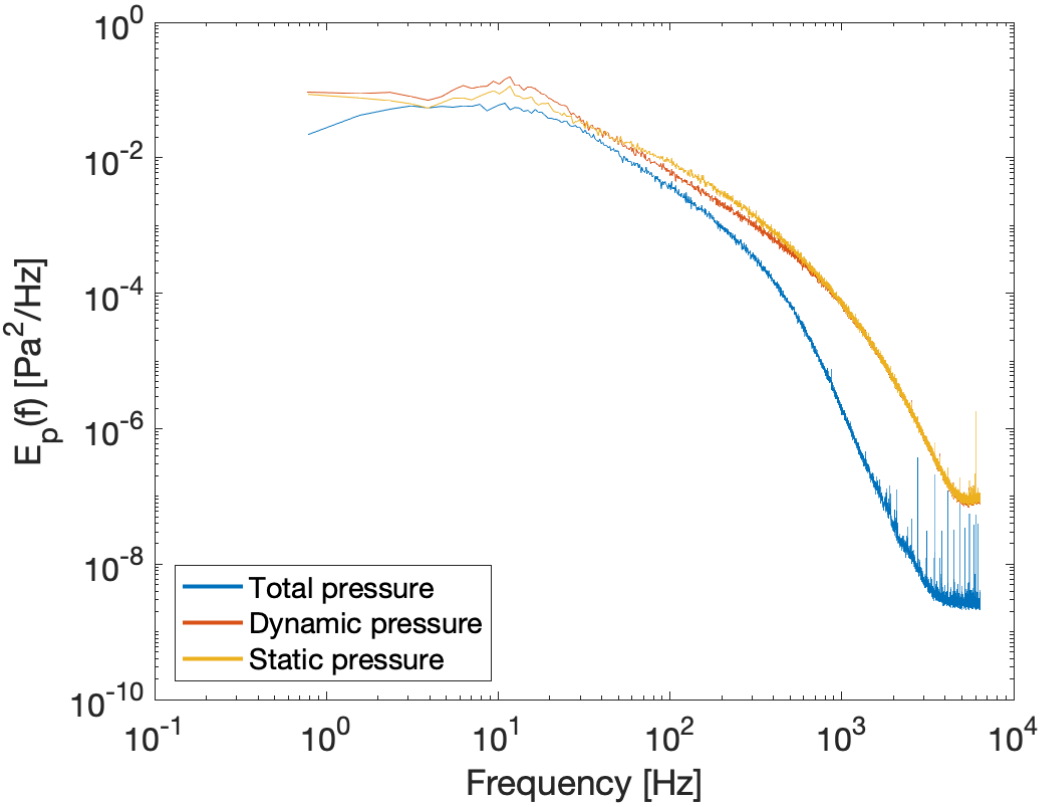

Figure 18: Total, dynamic, and static pressure spectra.

Since the static pressure fluctuation in equation (19) is dependent upon both the total and dynamic pressure fluctuations, the drift of total pressure away from dynamic pressure results in the static pressure being dominated by the latter. If the magnitude of the total pressure fluctuations becomes significantly lower than the magnitude of dynamic pressure fluctuations, the resultant values of static pressure fluctuations will become very closely related to the values of the dynamic pressure fluctuations. The drift of total pressure fluctuations away from dynamic pressure fluctuations poses the problem that the static pressure fluctuations are not properly resolved as they are extremely reflective of the dynamic pressure fluctuations.

Figure 19 shows the plots for the velocity and static pressure spectra. When compared to the spectra recorded by Tsuji & Ishihara [3], as shown in figure 1, it becomes apparent that there are discrepancies regarding the overall interactions between the velocity and static pressure spectra as

depicted in figure 19. Unlike Tsuji & Ishihara's plots, the slopes of -5/3 for velocity and -7/3 for pressure are not observed in the inertial range.

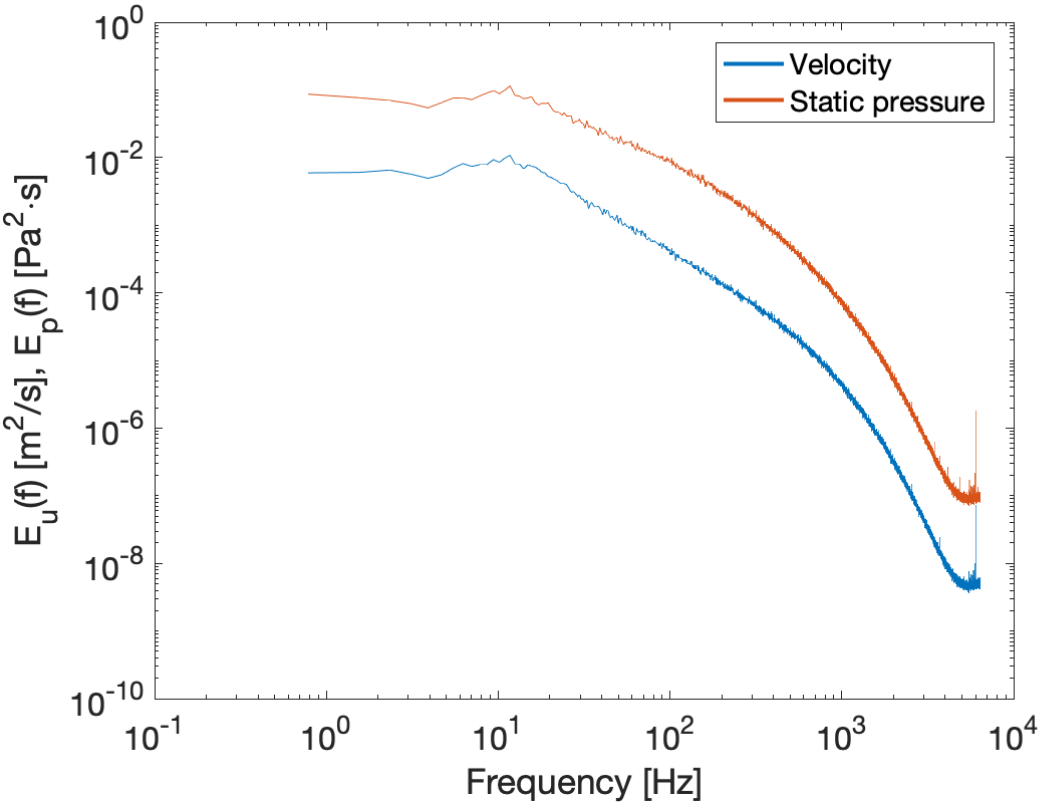

Figure 19: Velocity and static pressure spectra.

While an improved SNR was observed in the indirect approach to measuring static pressure, the inconsistencies with literature consequently mean that this method cannot be established as being reliable with regards to the acquired data. It is possible that the relatively large size of the microphone (especially when compared to the much smaller diameter of the static pressure probe) may be resulting in an excessively large correlation between the induced static pressure and velocity fields. This method, therefore, requires further investigation and more simultaneous velocity and pressure data should be recorded under varying flow conditions to draw conclusions.

4 CONCLUSION

4.1 Summary

Performance enhancement of the static-pressure probe was attempted through various methods and techniques. Physical enhancements consisting of signal conditioning, tube length alterations, flow conditioning, vibration reduction, and increasing the turbulence signal were applied to increase the probe's SNR.

Improvements in the SNR of the probe were observed by using larger gains on the signal conditioner. Low energy fluctuations in the inertial and dissipation ranges were better resolved with a gain of 100 as opposed to gains of 1 or 10. The next attempt at increasing the SNR by using a shorter tube length was less effective. Only minor changes in the quality of the spectra were observed. It then became apparent that the length of the tube had negligible effects on noise reduction or on the shape of the recorded spectra.

A successful method of reducing the noise in the data was the introduction of the probe into a planar jet. External flow conditions proved to be more optimized for microphone measurements than conditions present in internal flows, which are often contaminated by noise resulting from wall vibrations and fan noise reflecting off the walls. Indeed, less noise was observed when the pressure spectra were recorded in the planar jet at the channel exit than when the data was recorded inside of an enclosed wind tunnel. Noise reduction in this condition was further complimented by the shortening of the rod connecting the probe to its base, which consequently reduced the probe's vibrations and lead to improvements in the SNR.

As opposed to noise reduction, increasing the turbulence signal by changing the fan speed also resulted in successive improvements in spectral quality with increasing fan speeds. While the fan speed produced high peaks in the observed spectra, the resultant spectra depicted an improved SNR.

Contrasting the results achieved by physical enhancements, however, the method of digital

filtering did not result in improved SNR of the static-pressure measurements. This may have been due primarily to the (non-two-dimensional) nature of the noise where the data was recorded, and thus the algorithm was ineffective at isolating the noise embedded within the data.

Finally, the alternate method involving simultaneous velocity and pressure measurements could not be credited with providing reliable data, as it was observed that the static pressure was extremely reflective of the dynamic pressure measurements. This effect became more dominant when the spectrum for total pressure drifted further away from the dynamic pressure spectrum. For these reasons, this technique requires further validation.

4.2 Future Work

With regards to future work to be done in this area, the first and foremost parameter to be explored should be the replacement of the condenser microphone with a piezo-resistive transducer. The latter provides voltage differences as a result of its material properties, as opposed to the motion of the diaphragm for the former. As Tsuji & Ishihara stated [3], a piezo-resistive transducer should be used for measurements in the case where $R_\lambda > 600$.

New designs for the static-pressure probe should also be explored to test the effects of the external shape of the probe on the acquired data. This would require manufacturing of new parts for the assembly, and the effects of using materials other than stainless steel can thus also be tested. A more rigid material for the tube of the probe should be used as opposed to the stainless-steel tube used for the tested design.

A total pressure probe proposed by Naka & Obi [14] should be constructed to increase the reliability of the simultaneous velocity and pressure measurement technique. The design for the probe is proposed in figure 20. It is evident from the design of this probe that it offers a higher spatial resolution than using a condenser microphone inserted into the flow. This might factor into the relatively unreliable data recorded in section 3.3. The smaller pressure probe diameter could also lead to less interference between the hot-wire probe and the pressure probe.

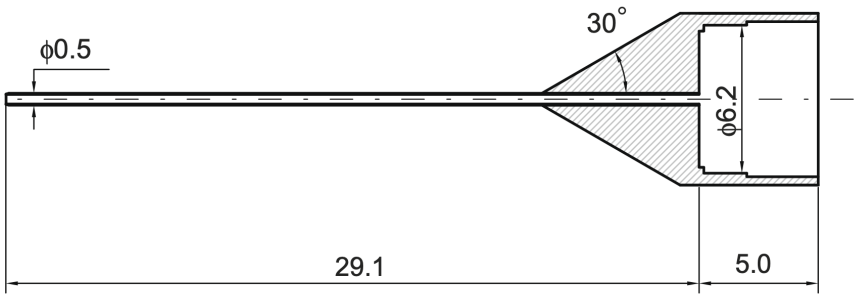

Figure 20: Schematic of a total pressure probe proposed by Naka & Obi [14] .

Appendix

A1 Uncertainty Analysis

In this section, an uncertainty analysis is performed for measurements acquired using the static pressure probe and hot-wire anemometry. Measurements made with the condenser microphone are subject to error originating from the microphone, the signal conditioner, and the data acquisition system. The relative standard uncertainty associated with these equipment can be found in the manuals provided by the manufacturer [6, 15]. The error originating from the DAQ board can be found using the equation [16]:

$$\text{uncertainty} = \left(\frac{1}{\sqrt{3}} \frac{1}{P} \frac{\partial P}{\partial E} \frac{E_{DAQ}}{2^n} \right) \times 100\%,$$

where P is the lowest pressure recorded, $\partial P/\partial E$ is the sensitivity of the microphone, E_{DAQ} is the voltage span (10 V) used to measure the data, and n is the number of bits (16) of the data acquisition system [17].

Source of error	**Relative standard uncertainty**
Microphone sensitivity	0.58%
Microphone frequency response	0.0012%
Signal conditioner resolution	0.02%
DAQ board resolution	0.000012%
Probe positioning	negligible

Table 1: Sources of error for pressure measurements.

Table 1 lists the errors associated with each of the components used for pressure data acquisition. The total relative expanded uncertainty can be calculated by combining the error contribution

from each source and using propagation of uncertainties given by the equation [16]:

$$\text{Total uncertainty} = 2\sqrt{(\text{uncertainty})_1^2 + (\text{uncertainty})_2^2 + ...}$$

A coverage factor of two is assumed to provide a confidence level of 95%. For pressure measurements, the total expanded uncertainty is 1.16%.

Velocity measurements are prone to errors originating from calibration curve fitting of the hot-wire, as well as temperature readings taken for calibration [17]. Error associated with the anemometer can be assumed to be negligible, as the constant temperature anemometer exhibits low drift and low noise, in addition to good repeatability. Temperature readings taken for hot-wire calibration are also subject to error. Sources of error for velocity measurements are summarized in table 2.

Source of error	**Relative standard uncertainty**
Calibration curve fit	1.3%
Calibration equipment	1%
Temperature measurements	0.33%
DAQ board resolution	0.015%
Anemometer	negligible
Probe positioning	negligible
Ambient humidity and pressure variations	negligible

Table 2: Sources of error for velocity measurements.

Once again assuming a coverage factor of two for a confidence level of 95%, the total expanded uncertainty for velocity measurements is 3.3%.

A2 Computer Code

A2.1 Optimal Digital Filtering (MATLAB)

Listing 1: main.m

```
%% Read the files and allocate variable names
file1 = '940_Long_175Honey.08aug2019.txt';
file2 = '940_Long_175Honey.31jul2019.txt';

frequency = 20000;
num_samples = 8192;
num_blocks = 200;

filename = fullfile(file1);
TL = readtable(filename,'Format','%f%f');
d_n = TL{:,2};
freq1 = TL{:,1};

filename = fullfile(file2);
TL2 = readtable(filename,'Format','%f%f');
x_n = TL2{:,2};
freq2 = TL2{:,1};

%% Calculate the auto and cross-correlations
R_auto = Autocorrelation_Calculator2(num_samples, x_n);
R_cross = Cross_correlation_Calculator2(num_samples, x_n, d_n);

%% Setup the R and g matrices
R = zeros(num_samples, num_samples);
g = R_cross;

for lv1 = 1:num_samples
```

```
    lv3 = 1;
    for lv2 = lv1:num_samples
        R(lv1,lv2) = R_auto(lv3);
        lv3 = lv3 + 1;
    end
end

for lv2 = 1:num_samples
    lv3 = 1;
    for lv1 = lv2:num_samples
        R(lv1,lv2) = R_auto(lv3);
        lv3 = lv3 + 1;
    end
end

f = R\g; %Solve for the filter coefficients
y_n = FIR_Filter(f, x_n); %Apply the filter coefficients
e_n = (d_n - y_n); %Calculate the filtered signal
```

Listing 2: FIR_Filter.m

```
function [y_n] = FIR_Filter(f, x_n)

N = length(f);
y = conv(x_n, f); %Convolution of filter coefficients
y_n = y(1:N);

end
```

A2.2 Static Pressure (from Total Pressure & Velocity) (MATLAB)

Listing 3: main.m

```
file1 = '432RPM_PV_43_5cm.06nov2019.txt';

filename = fullfile(file1);
TL = readtable(filename,'Format','%f%f');

%% Calibration constants
a = 4.761;
b = 0.3886;
c = 9.619;

%% Read pressure and velocity from the table
V = TL{:,1};
P = TL{:,2};

rho = 1.225;

%% Calculations

V = V + 4.1417; %Add the mean voltage back in
P = P*0.01; %Gain
P = P/0.001; %Sensitivity
P0 = P;

V = ((V.^2 - c)/a).^(1/b); %Convert voltage into velocity
U = mean(V);%Mean velocity

P_d = rho*V.^2/2; %Dynamic pressure
P_d_fluc = P_d - mean(P_d); %Fluctuating dynamic pressure

```

```
30 u = V-U; %Fluctuating velocity
31
32 u_square = u.^2;
33 u_square_mean = mean(u_square);
34
35 Ps = P0 - rho/2*(2*U.*u + u.^2 - u_square_mean); %Static pressure
```

References

[1] H. Tennekes and J. L. Lumley, *A First Course in Turbulence*. Cambridge, Massachusetts, and London, England: The MIT Press, First ed., 1972.

[2] S. B. Pope, *Turbulent Flows*. Cornell University, New York: Cambridge University Press, First ed., 2000.

[3] Y. Tsuji and T. Ishihara, "Similarity scaling of pressure fluctuation in turbulence," *Physical Review E*, vol. 68, August 2003.

[4] K. Toyoda, R. Hiramoto, and Y. Shirahama, "Measurements of fluctuating static pressure in a rectangular jet," *Fluid Measurement and Instrumentation*, vol. 211, pp. 13–18, 1995.

[5] T. Kawata, *Simultaneous measurement of fluctuating velocity and pressure in complex turbulent shear flow associated with large-scale vortex structure*. PhD thesis, School of Science for Open and Environmental Systems, Keio University, August 2014.

[6] *1/4" Pressure Filed Microphone & Preamplifier*. PCB Piezotronics, 2019.

[7] *Microphone Handbook*. PCB Piezotronics, 2019.

[8] "Measuring sound with microphones," March 2019. Accessed on: Nov.12, 2019. [Online]. Available: https://www.ni.com/en-my/innovations/white-papers/13/measuring-sound-with-microphones.html.

[9] *General Signal Conditioning Guide*. PCB Piezotronics, 2019.

[10] Y. Shirahama and K. Toyoda, "Development of the probe to measure static-pressure fluctuations (application to the measurements of jets)," *Transactions of the Japan Society of Mechanical Engineers Series B*, vol. 59, pp. 3381–3387, November 1993.

[11] N. Agarwal and R. Simpson, "A new technique for obtaining the turbulent pressure spectrum from the surface pressure spectrum.," *Journal of Sound and Vibration*, vol. 135, pp. 346–350, December 1989.

[12] A. Naguib, S. Gravante, and C. Wark, "Extraction of turbulent wall-pressure time-series using an optimal filtering scheme," *Experiments in Fluids*, vol. 22, pp. 14–22, June 1996.

[13] W. H. Press, S. A. Teukolsky, W. T. Vetterling, and B. P. Flannery, *Numerical Recipes in C*. New York, NY: Cambridge University Press, Second ed., 2002.

[14] Y. Naka and S. Obi, "Velocity-pressure correlation measurements in complex free shear flows," *International Journal of Heat and Fluid Flow*, vol. 30, pp. 411–420, January 2009.

[15] *Model 480E09 1-Channel, battery-powered, ICP® sensor signal conditioner, gain x1, x10, Installation and Operating Manual*. PCB Piezotronics, 2016.

[16] F. E. Jørgensen, *How to measure turbulence with hot-wire anemometers*. Dantec Dynamics, 2002.

[17] A. Berajeklian, "Simultaneous measurements of velocity and temperature in the heated wake of a cylinder with applications to the modeling of turbulent passive scalars," August 2010.